# Ultrahigh Thermoelectric Performance by Electron and Phonon Critical Scattering in $Cu_2Se_{1-x}I_x$

*Huili Liu, Xun Yuan, Ping Lu, Xun Shi,* Fangfang Xu, Ying He, Yunshan Tang, Shengqiang Bai, Wenqing Zhang,* Lidong Chen,* Yue Lin, Lei Shi, He Lin, Xingyu Gao, Xingmin Zhang, Hang Chi, and Ctirad Uher*

Besides the potentially great impact on efficient harvesting and conversion of waste industrial heat into electricity as well as providing a fully solid-state operational heat pump,[1,2] thermoelectricity has also attracted considerable interest by the electronic industry due to its potential to rapidly cool microprocessors and sensors, thus increasing their speed and capacity.[3–6] Applications of thermoelectrics in electronic industry require highly efficient materials with an exceptional figure of merit ($zT$) that would operate within a narrow temperature range near room temperature. Unlike the traditional applications in solid-state heat pumping and waste heat recovery that require a high TE performance over an extended regime of temperatures to maximize energy conversion efficiency, the rapid cooling devices for microprocessors and micro-power generators in wireless devices call only for a high TE efficiency within a relatively small temperature interval less than 30–50 degrees around or slightly above room temperature.[3–6] While recent advances in developing thermoelectric materials for power generation have resulted in $zT$ around 2 typically near 1000 K, room temperature applications of thermoelectricity are still hampered by the lack of materials having $zT$ above 1. Here we demonstrate a significantly improved thermoelectric performance by utilizing critical electron and phonon scattering that takes place during a continuous phase transition. Using iodine-doped $Cu_2Se$ where the critical phase transition temperature can be tuned to within a few tens of degrees around room temperature, we show that critical scattering greatly enhances the thermopower and strongly diminishes thermal conductivity, leading to a dramatic increase in $zT$ by a factor of 3–7 times culminating in $zT$ values of 2.3 at 400 K. This new mechanism provides great opportunities for $zT$ enhancement in materials displaying second-order phase transitions near ambient temperature and is appealing for a more extensive use of thermoelectrics in electronic industry.

Dr. H. Liu,[+] X. Yuan,[+] P. Lu, Prof. X. Shi, F. Xu, Y. He, W. Zhang, L. Chen
State Key Laboratory of High Performance Ceramics and Superfine Microstructure
Shanghai Institute of Ceramics
Chinese Academy of Sciences
1295 Dingxi Road, Shanghai, 200050, China
E-mail: xshi@mail.sic.ac.cn; wqzhang@mail.sic.ac.cn; cld@mail.sic.ac.cn
Dr. H. Liu, X. Yuan, P. Lu, Y. He
University of Chinese Academy of Sciences
Beijing, 100049,China
Prof. X. Shi, Mr. Y. Tang, Dr. S. Bai, L. Chen
CAS Key Laboratory of Energy Conversion Materials
Shanghai Institute of Ceramics
Chinese Academy of Sciences
1295 Dingxi Road, Shanghai, 200050, China
Dr. Y. Lin, L. Shi
Hefei National Laboratory for Physical Sciences at the Microscale
University of Science and Technology of China
Hefei, Anhui, 230026, China
Prof. H. Lin, X. Gao, Dr. X. Zhang
Shanghai Synchrotron Radiation Facility
Shanghai Institute of Applied Physics
Chinese Academy of Sciences
239 Zhangheng Road, Shanghai, 201204, China
Dr. H. Chi, Prof. C. Uher
Department of Physics
University of Michigan,
Ann Arbor, Michigan 48109, USA
[+]These authors contributed equally to this work.

**DOI: 10.1002/adma.201302660**

The energy conversion efficiency in TE technology is mainly limited by the materials' performance, which is described by the dimensionless TE figure of merit $zT$.

$$zT = \frac{S^2 T}{\rho \kappa} \tag{1}$$

The figure of merit depends, apart from the absolute temperature $T$, on three transport parameters: thermopower $S$ (Seebeck coefficient), thermal conductivity $\kappa$, and electrical resistivity $\rho$. The three transport coefficients are strongly inter-dependent (see Equation (1)), making the design of high $zT$ materials a very challenging task. Currently, the bulk materials with $zT$ above 2 have only been reported at fairly high temperatures near 1000 K in a few nano-structured materials.[7,8] The room temperature commercial $Bi_2Te_3$-based TE materials have a maximum $zT$ much less than 2.[2] Therefore, there is an urgent need to develop high performance TE materials for near room temperature applications such as providing rapid and efficient cooling of microprocessors and micro-generators for wireless devices.

The current successful strategies for enhancing the performance of TE materials focus mostly on the reduction of the thermal conductivity by incorporating nanometer-scale inclusions,[7–13] rattlers,[14] or the liquid-like state.[15] In principle, there is a limiting value which the lattice thermal conductivity ($\kappa_{min}$) can reach in solid materials[16] although the recent work suggests the $\kappa_{min}$ in materials with a liquid-like state could be even smaller due to an additional reduction of the specific heat.[15] For the current state-of-the-art TE materials such as

$Bi_2Te_3$,[2] PbTe,[17] or for multiple-filled skutterudites,[18] the lattice thermal conductivities ($\kappa_L$) are very low and some of them have approached the $\kappa_{min}$ value. In this case, any further enhancement in $zT$ must come from improvements in the Seebeck coefficient, $S$. This, however, is a truly challenging task since $S$ is determined by the electronic properties in a very narrow window of energy within a few $k_BT$ around the Fermi level ($E_F$), where $k_B$ stands for the Boltzmann constant. Only a few successful examples of enhancing the Seebeck coefficient have been reported and they depend either on the distortion of the electronic density of states by forming band-resonant states such as Tl does in PbTe[19] or on the presence of unbalanced spin and orbital degrees of freedom among magnetic ions with different charge states in cobalt oxides.[20]

Here, we show that the Seebeck coefficient and thermal conductivity can be significantly increased and decreased respectively by critical scattering of electrons and phonons during the second-order phase transition in $Cu_2Se$, leading to $zT$ values dramatically improved above 2 within a range of dozens of degrees around room temperature. Elemental doping can easily tune (lower) the peak temperature of $zT$, providing a great flexibility for applications such as cooling of microprocessors. The basis in this work is the additional electron and phonon scattering by fluctuations in the sample density, concentration, structure, and correlations of sample density-concentration induced by thermal fluctuation when the temperature approaches the critical phase transition point $T_C$, which could strongly scatter carriers and phonons in the form of a combined critical scattering. The effect of the electron critical scattering on the Seebeck coefficient can be described by the Mott expression[21] given in Equation (2).

$$S = \frac{\pi^2 k_B^2 T}{3q}\left\{\frac{d[\ln(\sigma(E))]}{dE}\right\}_{E=E_F} = \frac{\pi^2 k_B^2 T}{3q}\left\{\frac{dn(E)}{ndE} + \frac{d\mu(E)}{\mu dE}\right\}_{E=E_F} \quad (2)$$

Here $q$ is the carrier charge and $\mu(E)$ the carrier mobility, which is determined by the relaxation time $\tau(E)$ and the carrier effective mass $m^*$ ($\mu(E) = q\tau(E)/m^*$). In addition to the normal carrier scattering in material phases, the electron critical scattering during the phase transition can strongly change $\mu(E)$ and its energy-dependence, and thereby provide a possibility for greatly enhancing the thermopower. In an element-doped TE semiconductor $Cu_2Se$, such investigations led to a series of values of $zT$ above 1 around room temperature and the highest $zT$ in excess of 2.3 at 400 K (**Figure 1**) by bringing into play critical phonon scattering.

$Cu_2Se$ is a good TE material at high temperatures with very low thermal conductivity on account of a liquid-like state of Cu ions.[15,22,23] It undergoes a structural transition from a non-cubic to the cubic phase upon heating the sample and therefore represents an excellent example for this study as it offers an exploration of the influence of critical scattering during the phase transition. Using the newly developed measurement equipment for electrical resistivity and thermopower (see Supporting Information) and laser flash method, the detailed TE transport measurements were carefully carried out to see

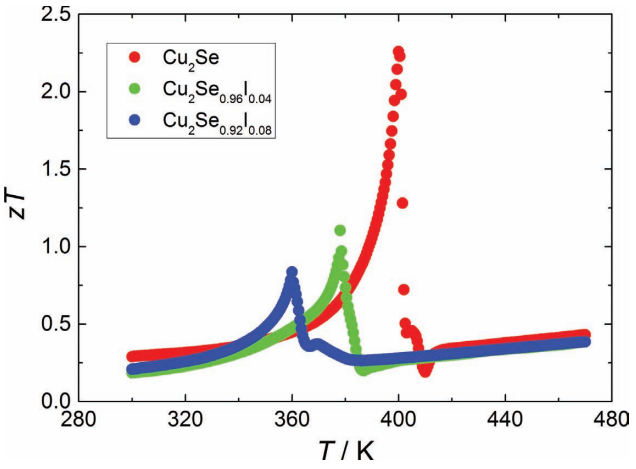


**Figure 1.** $zT$ curves for iodine-doped $Cu_2Se$, which show hugely increased values due to electron and phonon critical scattering during the phase transition.

accurately the physical trends during the phase transition in iodine-doped $Cu_2Se$ and the results are shown in **Figure 2**a–c. Monotonous changes in $S$, $\rho$, and $\kappa$ are observed in both $\alpha$- and $\beta$-phases. However, we detect abnormal transitions in transport coefficients in the interval 340~410 K. The Seebeck coefficient and the electrical resistivity sharply increase by a factor between 2 and 4, while the thermal conductivity is rapidly reduced when $T$ is approaching $T_C$. $Cu_2Se$ is a typical p-type conductor due to the deficiency of Cu in the crystal lattice. Iodine in the lattice of $Cu_2Se$ provides one extra electron and thereby acts as n-type doping. This is consistent with the observed increased electrical resistivity in iodine-doped samples shown in Figure 2b. In addition, doping by iodine shifts the transition temperature $T_C$ to lower temperatures without significantly changing the character of the phase transition. A significant change in TE properties is observed in the doped samples when $T_C$ is lowered from 400 K to 360 K. Based on the measured individual properties, the $zT$ quickly improves to values above 1 during the phase transition (Figure 1), a factor of 3 to 7 times larger than the figure of merit when the structure is outside of the transition region.

To further confirm the significantly improved $zT$ values during the phase transitions, a device with a single-pair of legs was constructed to measure the cooling ability as this is directly determined by the materials' $zT$ values (see the details in Supporting Information). Here, $Cu_2Se$ is used as the p-type leg, and Yb single-filled skutterudite is chosen as the n-type leg because its $zT$ value (about 0.2-0.4 below 400 K)[18] matches those of the normal α- and β-phases of $Cu_2Se$. The averaged $zT$ values of $Cu_2Se$ are around 0.6 between 300 and 400 K, two times larger than those of the normal $\alpha$- and $\beta$-phases. The maximum temperature drop ($\Delta T$) achieved with respect to the temperature of the cold junction ($T_{CJ}$) for various currents ($I$) at different cold junction temperatures is shown in Figure S9. The $\Delta T$ values in the phase transition region are significantly higher than those of normal α- and β-phases. The hugely enhanced cooling ability during the phase transition is further verified by the values of $\Delta T/T_{CJ}$ (see Supporting Information) when the current is small, the data shown in Figure 2d. For a range

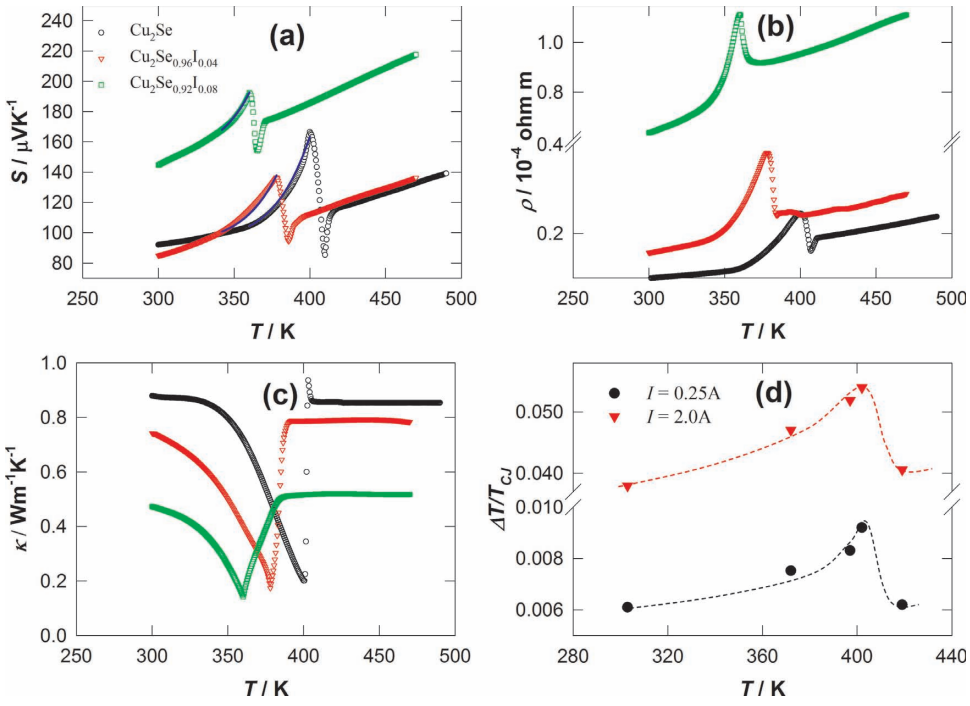


**Figure 2.** Temperature dependence of thermoelectric properties in iodine-doped $Cu_2Se$ materials and performance of the cooling device. a) thermopower ($S$), b) electrical resistivity ($\rho$), c) thermal conductivity ($\kappa$), and d) $\Delta T/T_{CJ}$ vs temperature in $\pi$-shape device where $\Delta T$ is the dropped temperature from the cold junction side ($T_{CJ}$). Solid lines in Figure 2a are calculated using Equation (3). Dashed lines in Figure 2d are guides to the eyes.

of small currents, the relationship between ($\Delta T/T_{CJ}$) and temperature shows a similar trend as does $zT$ with the values significantly improved during the phase transition. The maximum enhancement is more than 50% for the device with only one leg benefiting from critical scattering. These cooling ability measurements of the device are fully consistent with the measured thermoelectric properties.

The abnormal TE properties in iodine-doped $Cu_2Se$ during the phase transition could be well explained by the presence of electron and phonon critical scattering in addition to the usual scattering processes. The critical scattering is tightly associated with the crystal structures of $\alpha$-phase and $\beta$-phase, and the structure variation during phase transitions. Different from the high temperature cubic $\beta$-phase of high symmetry, the low temperature $\alpha$-phase of low symmetry in $Cu_2Se$ is complicated and its crystal structure is not yet fully determined. Starting from the first principles calculations, one possible crystal configuration of $Cu_2Se$ is shown in **Figure 3**a (see the details in Supporting Information). The high temperature cubic phase has regular two copper layers between Se layers (see the marked red region). Upon undergoing the transition into the low temperature $\alpha$-phase, the copper layers above or below the red region are completely moved into the red region resulting in a new structure. There are no copper ions located between the Se layers next to the red frame. As a result, the high temperature cubic phase is transferred to a layered structure at room temperature, where the layers are interconnected by Se–Se bonds.

This layered structure is supported by the X-ray diffraction analysis of the ingot before Spark Plasma Sintering (SPS) (shown in Figure 3b). Only peaks corresponding to (0 0 n) planes are displayed at room temperature, a typical pattern of a layered material shown in Figure 3a (left one). However, at 420 K, all room temperature peaks have disappeared and only cubic peaks are observed, consistent with the structure shown in the right-hand diagram of Figure 3a. High resolution transmission electron microscopy further confirmed the proposed layered structure of the $\alpha$-phase (Figure 3c–e). Atom-resolved high-angle annular dark-field (HAADF) Z-contrast image at room temperature clearly visualizes gathering of Cu into one Se interlayer while leaving interlayer at its either side empty of Cu. The experimental and calculated diffraction patterns are consistent and reflect a layered structure by noting the doubled interplanar spaces of a {111} cubic plane owing to alternating segregation of Cu atoms. Clustering of Cu within a Se interlayer suggests existence of Cu-Cu bonding. This has also been evidenced by electron energy-loss spectroscopy (EELS) analysis (Figure S5).

According to the literature[15] and our own Differential Scanning Calorimetry (DSC) measurement, the transition temperature $T_C$ for $Cu_2Se$ is near 400 K. (Figure S1, Supporting Information). Doping by element iodine shifts $T_C$ toward room temperature (see Supporting Information). Figure 3f shows the calculated energies of transformation path during the phase transformation. Very smooth changes in energy demonstrate that there are no energy barriers, a behavior typical of the second-order phase transition. This is further confirmed by High-Temperature X-Ray Diffraction (HTXRD) and Synchrotron Radiation Light Source (SRLS) measurements. A gradual and continuous phase transition shown in Figure 3g is observed

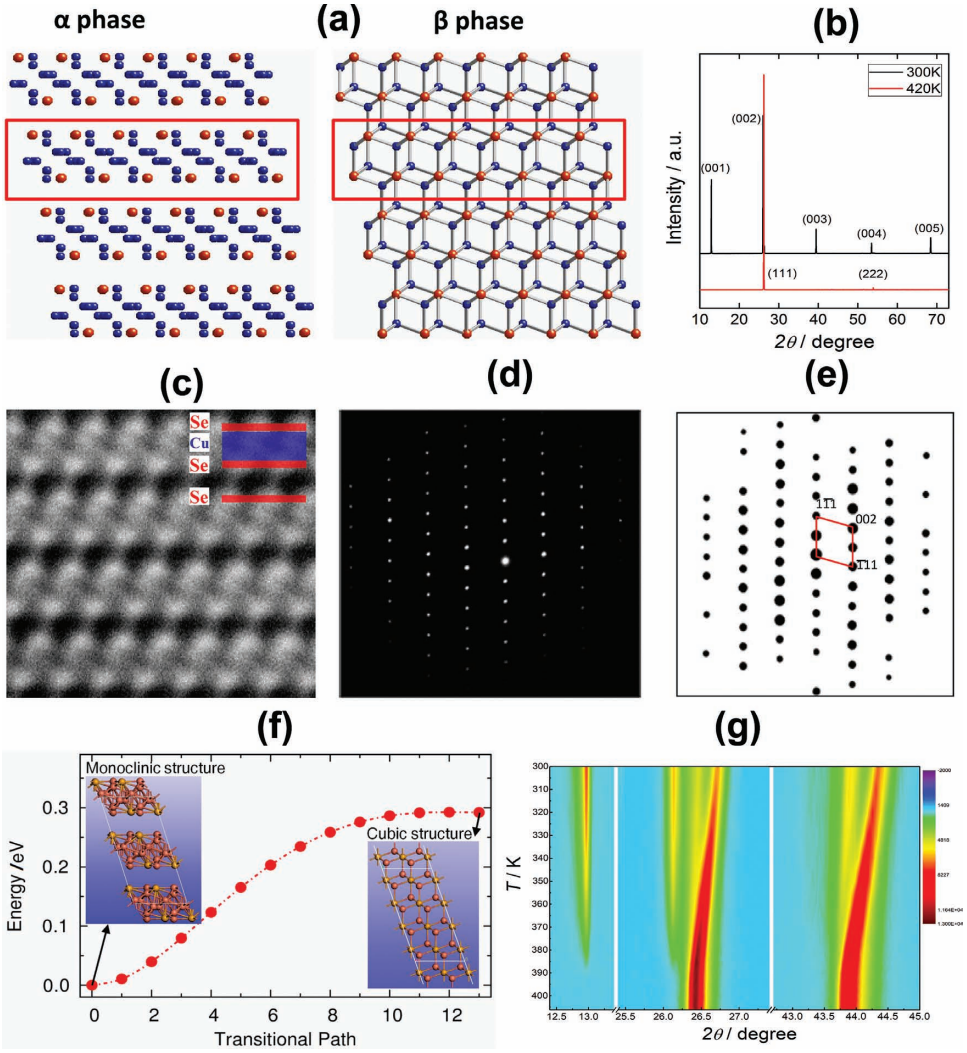


**Figure 3.** Structure aspects of $Cu_2Se$. a) Crystal structures of room temperature $\alpha$-phase (left) and high temperature cubic $\beta$-phase (right) in $Cu_2Se$. Cu ions are randomly distributed at 8c and 32f sites in the cubic β-phase. Here they are fixed at 8c sites in the right-hand side picture in order to simplify the figure. b) X-ray diffraction peaks of $Cu_2Se$ ingot before SPS, showing different crystal structures for room and high temperature phases. c) Atom-resolved HAADF image at room temperature, where large bright dots refer to Se atoms and weak contrast among Se layers refer to Cu atoms. d) Experimental electron diffraction pattern of the monoclinic phase obtained from a micro-region in the ingot sample before sintering. e) Calculated electron diffraction pattern using the structure shown in Figure 3a (left one). The framed lattice in (e) refers to the primitive cubic structure in <110> direction. f) Calculated energies of the transition states during the phase transformation. g) HTXRD data collected on heating of $Cu_2Se$ powder from 300 K (top) to 410 K (bottom), showing the coalescence of the split peaks around 26.4–26.7° and 44.0°, and the disappearance of the extra peaks around 12.9° and 26.5° as the lower-symmetry α-phase transforms to the higher-symmetry cubic β-phase.

when the sample is heated to high temperatures. Above 400 K, the low temperature α-phase is completely transformed to the cubic β-phase. SRLS measurements (see Figure S2) give similar results showing how the peak of the α-phase at 26.15° steadily weakens and finally disappears, while the peak around 26.4° gradually shifts left and finally transits to the cubic peak.

The character of the second-order structural phase transition results in extremely large fluctuations in the sample density, concentration, structure, and correlated sample density-concentration induced by thermal fluctuation at $T_C$,[24] and thus could lead to extremely large electron and phonon critical scattering. The lattice thermal conductivities during phase transitions (shown in Figure S7) are significantly lowered compared to the normal phases. In addition, the effect of the electron critical scattering on carrier mobility induced by the thermal fluctuations during the second-order phase transition in $Cu_2Se$ can be determined from the Hall and mobility measurements on $Cu_2Se$ (**Figure 4**a). In $\alpha$- and $\beta$-phases, the carrier mobility varies as $T^{-3/2}$, indicating the electron scattering is dominated by normal electron-acoustic phonon interactions. This is prevailing interaction in TE materials around room temperature. However, we detect a dramatically decreased mobility by a factor of up to four during the phase transition. The relationship between the mobility and temperature is also significantly altered from the normal acoustic phonon scattering and shows extremely large temperature dependence. This is fully

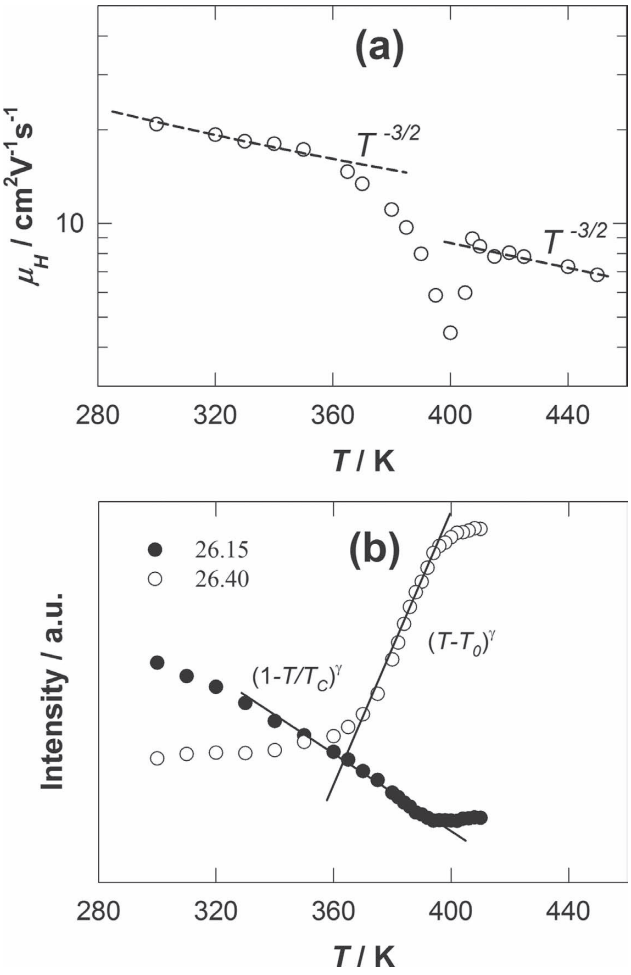


**Figure 4.** Temperature dependence of the intensity of peaks and carrier mobility in $Cu_2Se$. a) Carrier mobility during the process of phase transitions. b) Peak intensity around 26.15° and 26.40° of the $\alpha$-phase. During the phase transition, variations of the intensity are given by formulas inserted in Figure 4b.

consistent with the ideal characteristic of electron critical scattering where it displays extremely large temperature dependence when $T$ approaches $T_C$.

The impact of this critical scattering on electrical transport could be judged from the intensity variation measured by HTXRD and shown in Figure 4b. The intensity of peaks between 26° and 27° shown in Figure 3g is presented because it covers both the increasing and decreasing peak intensities when the sample is heated and the structure changes from the α-phase to the β-phase during the phase transition. The peak of the α-phase at around 26.15° is diminished and the peak of the $\beta$-phase near 26.4° is increased when $T$ approaching $T_C$. The corresponded peak intensities vary as $(1\text{-}T/Tc)^\delta$ for the $\alpha$-phase and $(T\text{-}T_0)^\delta$ for the $\beta$-phase where $\delta$ is a constant with the value of about 1 by fitting the experimental data in Figure 4b, where $T_0$ is the onset temperature of the phase transition. These relationships thus could be used to describe the weights of normal and critical electron scattering during the second-order phase transition in iodine-doped $Cu_2Se$.

For a material with two distinct carrier scattering mechanisms present,[25] the total $\rho$ has two contributions from the normal and critical electron scattering with the electrical resistivity $\rho_c$ of the maximized fluctuated phase at $T_C$ four times larger than the value of the normal phase at $T_0$. The expression for the thermopower above the Debye temperature can be derived from Equation (2) for a material with both normal and critical electron scattering, the approach used to explain the abnormal thermopower near $T_C$ in metal alloys.[26] Here, in semiconducting iodine-doped $Cu_2Se$, the thermopower is given by Equation (3) which includes weights of normal and critical electron scattering.

$$S = S_0 + AT\left(\frac{T-T_0}{T_C-T_0}\right)^\gamma \frac{\rho}{\rho_C} \quad (3)$$

Calculated transport parameters (solid lines in Figure 2a) are fully consistent with the experimental data for all samples. The fitting parameters are given in Table S3. Thus, starting with the Mott expression, Equation (3) gives a nice connection between $S$ and $\rho$ that enables to describe the abnormal electrical transport, especially the rapid enhancement of the thermopower, during the phase transition when iodine-doped $Cu_2Se$ is influenced by electron critical scattering.

The use of electron and phonon critical scattering in enhancing $zT$ goes beyond the traditional ideas and approaches of improving TE performance with the possibility of realizing ultrahigh $zT$ values. It takes an advantage of significant optimization of electrical and thermal transport properties in addition to the material's intrinsic physical properties such as its electronic band structure. Using this new approach, charge carriers and phonons can be strongly scattered to achieve very high thermopower and low thermal conductivity, and thereby the exceptional thermoelectric performance. Iodine-doped $Cu_2Se$ with its large temperature dependent structural transition illustrates an example how to achieve $zT$ of 2.3 near room temperature by relying on critical scattering. Abnormal TE properties observed during phase transitions have also been reported recently in other metal chalcogenides.[27] With exceptionally high values of the figure of merit observed in the phase transition region and with the ability to tune the phase transition temperature by doping, we can expect a proliferation of applications where these new phase transition thermoelectrics would serve as powerful solid-state heat pumps or power generators within a narrow (a few tens of degrees) temperature range around room temperature. Cooling microprocessors or utilizing miniature thermoelectric generators to power wireless sensors are just two important applications.

## Experimental Section

Polycrystalline $Cu_2Se_{1-x}I_x$ samples were prepared by melting Cu (shot, 99.999%, Alfa Aesar), Se (shot, 99.999%, Alfa Aesar), and CuI (powder, 99.998%, Alfa Aesar) in Pyrolytic Boron Nitride (P-BN) crucibles enclosed in a fused silica tube at 1423 K for 24 hours under vacuum. The melt was slowly cooled down to 923 K in 50 hours and was rested at 923 K for 5 days, and finally being slowly cooled down to room temperature in 50 hours. The resulting ingots were ground

into fine powder in an agate jar and plunger and then sintered by spark plasma sintering (Sumitomo SPS-2040) at around 750 K under a pressure of 65 MPa. The bulk samples show random orientation distribuions of grains (see details in Supporting Information), suggesting isotropic TE properties. The thermal diffusivity ($D$) was measured using the laser flash method (Netzsch, LFA457) with a temperature step as small as less than 1 K. The density ($d$) was measured by Archimedes method. Thermal conductivity was calculated from $\kappa = D \times C_P \times d$ by taking the Dulong-Petit value for $C_p$. The enhanced cooling efficiency of thermoelectric device using $Cu_2Se$ shown in Figure 3d strongly implied that the Dulong-Petit value of $C_p$ should be used for the calculations of thermal conductivities during phase transitions. This is due to the fact that the additional heat enthalpy during phase transitions does not contribute to heat transfer because the energy is adopted and stored in materials' entropy. Hall coefficient measurements were performed at the University of Michigan. Differential Scanning Calorimetry (DSC) measurements were performed using the Netzsch DSC 200F3 apparatus to identify the materials' phase transition temperatures. TEM examination was performed on a JEM-2100F field-emission transmission electron microscope. Atom resolved HAADF images were acquired using a JEM-ARM200F Cs-corrected scanning transmission electron microscope. X-ray measurements were performed at the Shanghai Synchrotron Radiation Facility (SSRF) with a wavelength of 1.24 Å. The $2\theta$ values in Figure S2 were calibrated using a normal wavelength of 1.5406 Å. High-temperature X-ray diffraction (HTXRD) patterns were collected on heating the samples with a temperature step as small as 1 degree during the phase transition.

In order to accurately measure the thermopower and electrical resistivity during the phase transition, we developed a new system based on the thermal expansion equipment (Netzsch DIL 402C). Two pairs of R-type thermocouples, one heater, and two Ni electrodes were packaged into the chamber of the thermal expansion system. The electrical resistivity was measured by the standard four-probe method. The thermopower was calculated from the slope of the $\Delta V$ *vs.* $\Delta T$ curve upon applying power to a heater and keeping $\Delta T$ to no more than 2–3 K. The Seebeck voltage $\Delta V$ was measured with a Keithley nanovoltmeter and the data were corrected for the thermopower of Pt.[28] We also developed a program to automatically collect the data. We used a sample of multiple-filled skutterudite to test the measurement accuracy of this new system. The data are fully consistent with the literature values measured using Ulvac ZEM-3 system.[18] Finally, the temperature dependence of thermopower and electrical resistivity was measured under a very small temperature step (around 0.1 K) between 300 K and 500 K and the data collection took about one week for each sample. Hall measurements were even more tedious as one had to stabilize the temperature to perform magnetic field sweeps in both field directions.

## Supporting Information

Supporting Information is available from the Wiley Online Library or from the author.

## Acknowledgements

We thank Dr. G. Jeffrey Snyder for helpful discussions and BL14B1 XRD station of Shanghai Synchrotron Radiation Facility (SSRF). This work is supported by National Basic Research Program of China (973-program) under Project No.2013CB632501, National Natural Science Foundation of China (NSFC) under the No. 51222209, 11234012 and 51121064. C.U. and H.C. wishes to acknowledge the support of the Center for Solar and Thermal Energy Conversion, an Energy Frontier Research Center funded by the U.S. Department of Energy, Office of Basic Energy Sciences under Award No. DE-SC00000957 in their measurements of the Hall effect.

Received: June 10, 2013
Revised: August 5, 2013
Published online: September 10, 2013

[1] L. E. Bell, *Science* **2008**, *321*, 1457.
[2] G. J. Snyder, E. S. Toberer, *Nature Mater.* **2008**, *7*, 105.
[3] G. J. Snyder, J. R. Lim, C. K. Huang, J. P. Fleurial, *Nature Mater.* **2003**, *2*, 528.
[4] I. Chowdhury, R. Prasher, K. Lofgreen, G. Chrysler, S. Narasimhan, R. Mahajan, D. Koester, R. Alley, R. Venkatasubramanian, *Nat. Nanotech.* **2009**, *4*, 235.
[5] N. S. Hudak, G. G. A matucci, *J. Appl. Phys.* **2008**, *103*, 101301.
[6] J. Sharp, J. Bierschenk, H. B. Lyon, *Proceedings of the IEEE* **2006**, *94*, 1602.
[7] K. F. Hsu, S. Loo, F. Guo, W. Chen, J. S. Dyck, C. Uher, T. Hogan, E. K. Polychroniadis, M. G. Kanatzidis, *Science* **2004**, *303*, 818.
[8] K. Biswas, J. He, I. D. Blum, C. I. Wu, T. P. Hogan, D. N. Seidman, V. P. Dravid, M. G. Kanatzidis, *Nature* **2012**, *489*, 414.
[9] A. I. Hochbaum, R. Chen, R. D. Delgado, W. Liang, E. C. Garnett, M. Najarian, A. Majumdar, P. Yang, *Nature* **2008**, *451*, 163.
[10] R. Venkatasubramanian, E. Siivola, T. Colpitts, B. O'Quinn, *Nature* **2001**, *413*, 597.
[11] T. C. Harman, P. J. Taylor, M. P. Walsh, B. E. LaForge, *Science* **2002**, *297*, 2229.
[12] M. S. Dresselhaus, G. Chen, M. Y. Tang, R. G. Yang, H. Lee, D. Z. Wang, Z. F. Ren, J. P. Fleurial, P. Gogna, *Adv. Mater.* **2007**, *19*, 1043.
[13] B. Poudel, Q. Hao, Y. Ma, Y. Lan, A. Minnich, B. Yu, X. Yan, D. Wang, A. Muto, D. Vashaee, X. Chen, J. Liu, M. S. Dresselhaus, G. Chen, Z. Ren, *Science* **2008**, *320*, 634.
[14] B. C. Sales, D. Mandrus, R. K. Williams, *Science* **1996**, *272*, 1325.
[15] H. Liu, X. Shi, F. Xu, L. Zhang, W. Zhang, L. Chen, Q. Li, C. Uher, T. Day, G. J. Snyder, *Nature Mater.* **2012**, *11*, 422.
[16] D. G. Cahill, S. K. Watson, R. O. Pohl, *Phys. Rev. B* **1992**, *46*, 6131.
[17] Y. Pei, X. Shi, A. D. LaLonde, H. Wang, L. Chen, G. J. Snyder, *Nature* **2011**, *473*, 66.
[18] X. Shi, J. Yang, J. R. Salvador, M. Chi, J. Y. Cho, H. Wang, S. Bai, J. Yang, W. Zhang, L. Chen, *J. Am. Chem. Soc.* **2011**, *133*, 7837.
[19] J. P. Heremans, V. Jovovic, E. S. Toberer, A. Saramat, K. Kurosaki, A. Charoenphakdee, S. Yamanaka, G. J. Snyder, *Science* **2008**, *321*, 554.
[20] I. Terasaki, Y. Sasago, K. Uchinokura, *Phys. Rev. B* **1997**, *56*, 12685.
[21] N. F. Mott, E. A. Davis, in Eletronic processes in non-crystalline materials, (Eds: W. Marshall, D. H. Wilkinson), Clarendon Press, Oxford **1971**, Ch. 3.
[22] X. Xiao, W. Xie, X. Tang, Q. Zhang, *Chin. Phys. B* **2011**, *20*, 087201.
[23] B. Yu, W. Liu, S. Chen, H. Wang, H. Wang, G. Chen, Z. Ren, *Nano Energy* **2012**, *1*, 472.
[24] H. Liu, X. Shi, M. Kirkham, H. Wang, Q. Li, C. Uher, W. Zhang, L. Chen, *Mater. Lett.* **2013**, *93*, 121.
[25] G. S. Nolas, J. Sharp, H. J. Goldsmid, in Thermoelectrics: basic principles and new materials developments, (Eds: A. Zunger, R. M. Osgood Jr., R. Hull, H. Sakaki), Springer Verlag, New York **2001**, Ch. 2.
[26] G. A. Thomas, K. Kevin, R. D. Parks, *Phys. Rev. Lett.* **1972**, *29*, 1321.
[27] C. Xiao, J. Xu, K. Li, J. Feng, J. Yang, Y. Xie, *J. Am. Chem. Soc.* **2012**, *134*, 4287.
[28] N. Cusack, P. Kendall, *Proceedings of the physical society of London* **1958**, *72*, 898.